Forest Height Estimation by Means of TanDEM-X InSAR and Waveform Lidar Data

Roman Guliaev, Victor Cazcarra-Bes, Matteo Pardini, *Member, IEEE*, and Konstantinos Papathanassiou, *Fellow, IEEE*

***Abstract*—Model-based forest height inversion from Pol-InSAR data relies on the realistic parameterization of the underlying (vertical) radar reflectivity function. In the context of interferometric TanDEM-X measurements – especially in the global single pol DEM mode – this is not possible due to the limited dimensionality of the observation space. In order to overcome this, the use of lidar waveforms to directly approximate the TanDEM-X reflectivity is proposed. This allows the forest height estimation from a single, single polarimetric, bistatic TanDEM-X acquisition. In order to extend the proposed lidar-supported inversion schema to areas only partially covered or sampled by (waveform) lidar measurements, the use of a "mean" (vertical) reflectivity profile is further proposed. This "mean" reflectivity profile is defined by means of the eigenfunctions of the available set of lidar waveforms. Both approaches are demonstrated and validated using TanDEM-X and airborne waveform lidar data acquired in the framework of the AfriSAR 2016 campaign over the Lopé National Park, in Gabon.**

***Index Terms*—Forest height estimation, SAR interferometry, TanDEM-X, vertical radar reflectivity, waveform lidar.**

I. Introduction

FOREST height is one of the most important forest parameters in forestry along with basal area and tree species or species composition. Depending on the forest type, it provides more or less significant information on stand development and/or site index and describes more or less accurate forest inventory and development. Accordingly, forest height can be used, alone or together with other parameters, as an indicator for site-dependent timber production potential and is directly related to forest biomass through allometric relations. Furthermore, accurate forest height measurements allow conclusions on the successional state of a forest and can be used to constrain model estimates of above-ground biomass and associated carbon flux components. The distribution of forest heights within a stand can be further used to characterize the disturbance regime while high (spatial and temporal) resolution forest height maps can be used for detecting selective logging activities [1]–[4].

Being a standard parameter in forest inventories, forest height is hard to be measured on the ground and becomes harder with increasing forest height and density. In terms of remote sensing techniques, lidar configurations have been today established as the reference (in terms of vertical and spatial resolution and/or accuracy) for measuring forest height on local and regional scales [5]. However, the rather small footprints of spaceborne lidar configurations do not allow large-scale wall-to-wall forest height measurements with a reasonable temporal resolution.

The introduction of polarimetric SAR interferometry (PolInSAR) at the end of the 90s was a decisive step toward developing measuring forest height accurately at large scales [6]–[11]. Relying on the inherent sensitivity of the interferometric coherence to the vertical structure of volume scatterers combined with the potential of SAR polarimetry to characterize individual scattering processes, PolInSAR techniques have been established for accurate forest height estimation on large scales in the context of air- and spaceborne implementations [12]–[15]. However, when it comes to spaceborne repeat-pass implementations, the inherent presence of temporal decorrelation degrades the sensitivity of PolInSAR measurements to vertical scattering structure and limits the performance of PolInSAR inversion techniques [16]–[18].

Launched in 2010, TanDEM-X introduced a new era in spaceborne radar remote sensing allowing single-pass interferometric measurements from space in a bistatic configuration [19], [20]. The sensitivity of the interferometric TanDEM-X coherence to the vertical forest structure and especially to forest height initiated a large number of studies on forest height estimation from TanDEM-X InSAR data across all possible forest types and conditions [21]–[24]. The proposed estimation algorithms are regression as well as model-based where the second ones appear, in general, more robust and with a better performance.

For the model-based forest height estimation algorithms, two main approaches have been established [25]. The first one relies on dual-polarized TanDEM-X (interferometric) measurements and allows forest height estimation without any a priori information. The achieved performance is, in general, remarkably good as long as the forest conditions allow sufficient penetration to ensure the "visibility" of the whole (vertical) forest extent. At denser forest conditions, X-band's insufficient penetration capability leads to a systematic underestimation of taller stands.

Manuscript received November 22, 2020; revised January 25, 2021; accepted January 26, 2021. Date of publication February 11, 2021; date of current version March 24, 2021. This work was supported by the frame of a Joint Research project between DLR and NASA's Carbon Monitoring System (CMS) Program in support of NASA under Grant 80NSSC20K0023 to the University of Maryland. *(Corresponding author: Matteo Pardini.)*

Victor Cazcarra-Bes, Matteo Pardini, and Konstantinos Papathanassiou are with the Microwave and Radar Institute, German Aerospace Center DLR Oberpfaffenhofen, 82234 Wessling, Germany (e-mail: victor.cazcarrabes@dlr.de; matteo.pardini@dlr.de; kostas.papathanassiou@dlr.de).

Roman Guliaev is with the Microwave and Radar Institute, German Aerospace Center DLR Oberpfaffenhofen, 82234 Wessling, Germany, and also with the Institute of Environmental Engineering, Swiss Federal Institute of Technology (ETH) Zurich,, 8093 Zurich, Switzerland (e-mail: roman.guliaev@dlr.de).

Digital Object Identifier 10.1109/JSTARS.2021.3058837

Besides this, the limited availability of dual-pol TanDEM-X data limits this approach to local scale experiments/demonstrations.

The second approach relies on single-polarimetric TanDEM-X measurements and requires knowledge of the underlying topography. This constrains its application on flat terrain areas or areas where a digital terrain model (DTM) is available. But at the same time, the knowledge of the underlying topography also allows unbiased height estimates even if the "visibility" of the whole forest extent is not given. Finally, the fact that it requires interferometric measurements at a single polarization allows its implementation by means of the standard DEM mode of TanDEM-X enabling large-scale application globally.

The wide availability of lidar data triggered a number of attempts to use lidar data and/or lidar-derived products to compensate for the inherent underdetermination of the forest height inversion problem when addressed in terms of single-polarimetric TanDEM-X measurements. Besides the obvious approach to use the lidar derived DTM to directly enable the forest height inversion as discussed in the previous paragraph [25]–[29], lidar data have also been used to constrain the forest height inversion problem reducing, in this way, the dimensionality of the inversion problem [30]–[33].

An alternative approach of combining waveform lidar measurements and single-polarization TanDEM-X data for forest height inversion is proposed in the following. Sections II and III review the interferometric TanDEM-X measurements and the forest height estimation methodology and define the framework for combining the waveform lidar and the interferometric radar measurements. Section IV summarizes the main characteristics of waveform lidar measurements. In Section V, the experimental data used are described. Sections VI and VII provide the experimental demonstration and validation of the proposed approach discussing its main performance characteristics. Finally, in Section VIII, the established understanding and the achieved results are concluded.

II. Interferometric Measurements

The main InSAR measurement is the complex interferometric coherence $\tilde{\gamma}_{\mathrm{Obs}}(\vec{\mathrm{w}})$ formed by using the two images $\mathrm{s}_1(\vec{\mathrm{w}})$ and $\mathrm{s}_2(\vec{\mathrm{w}})$ acquired at a given polarization (indicated by the unit vector $\vec{\mathrm{w}}$) with a given spatial (and temporal) baseline [i.e., spatial (and temporal) separation]

$$\tilde{\gamma}_{\mathrm{Obs}}\left(\vec{\mathrm{w}}\right)=\frac{\left\langle \mathrm{s}_1\left(\vec{\mathrm{w}}\right)\mathrm{s}_2^{*}\left(\vec{\mathrm{w}}\right)\right\rangle}{\sqrt{\left\langle \mathrm{s}_1\left(\vec{\mathrm{w}}\right)\mathrm{s}_1^{*}\left(\vec{\mathrm{w}}\right)\right\rangle\left\langle \mathrm{s}_2\left(\vec{\mathrm{w}}\right)\mathrm{s}_2^{*}\left(\vec{\mathrm{w}}\right)\right\rangle}} \tag{1}$$

where $<\cdots>$ denotes the expected value. $\tilde{\gamma}_{\mathrm{Obs}}(\vec{\mathrm{w}})$ comprises several decorrelation contributions and can, therefore, be factorized as

$$\tilde{\gamma}_{\mathrm{Obs}}\left(\vec{\mathrm{w}}\right)=\tilde{\gamma}_{\mathrm{Tmp}}\left(\vec{\mathrm{w}}\right)\tilde{\gamma}_{\mathrm{Sys}}\left(\vec{\mathrm{w}}\right)\tilde{\gamma}_{\mathrm{Scat}}\left(\vec{\mathrm{w}}\right). \tag{2}$$

The first contribution is the so-called temporal decorrelation contribution $\tilde{\gamma}_{\mathrm{Tmp}}(\vec{\mathrm{w}})$ introduced by geometric and/or dielectric changes of the scatterers within the scene in the time interval between the two interferometric acquisitions. For the TanDEM-X bistatic mode, where one of the two satellites transmit and both satellites receive the scattered signal quasi simultaneously (with temporal baselines on the order of a fraction of a second), $\tilde{\gamma}_{\mathrm{Tmp}}\left(\vec{\mathrm{w}}\right)=1$.

The second term, $\tilde{\gamma}_{\mathrm{Sys}}(\vec{\mathrm{w}})$, comprises a wide range of decorrelation effects induced by the non-ideal SAR system and processing implementations. The most relevant system decorrelation contribution is the additive noise decorrelation $\gamma_{\mathrm{SNR}}(\vec{\mathrm{w}})$. Modeling the received signal to be composed by the scattering amplitude $\mathrm{a}(\vec{\mathrm{w}})$ and the noise amplitude $\mathrm{n}(\vec{\mathrm{w}})$, i.e., $\mathrm{s}\left(\vec{\mathrm{w}}\right)=\mathrm{a}(\vec{\mathrm{w}})+\mathrm{n}(\vec{\mathrm{w}})$, $\gamma_{\mathrm{SNR}}(\vec{\mathrm{w}})$ can be written as [11]

$$\gamma_{\mathrm{SNR}}\left(\vec{\mathrm{w}}\right)=\frac{1}{1+\mathrm{SNR}(\vec{\mathrm{w}})^{-1}}=\frac{\mathrm{A}\left(\vec{\mathrm{w}}\right)}{\mathrm{A}\left(\vec{\mathrm{w}}\right)+\mathrm{N}\left(\vec{\mathrm{w}}\right)}=\frac{\mathrm{A}\left(\vec{\mathrm{w}}\right)}{\mathrm{P}\left(\vec{\mathrm{w}}\right)} \tag{3}$$

where $\mathrm{SNR}(\vec{\mathrm{w}})=\mathrm{A}(\vec{\mathrm{w}})/\mathrm{N}(\vec{\mathrm{w}})$ is the signal-to-noise ratio, with $\mathrm{P}\left(\vec{\mathrm{w}}\right)=\mathrm{A}(\vec{\mathrm{w}})+\mathrm{N}(\vec{\mathrm{w}})$ is the received power, $\mathrm{A}\left(\vec{\mathrm{w}}\right)=|\mathrm{a}(\vec{\mathrm{w}})|^2$ is the scattered power, and $\mathrm{N}\left(\vec{\mathrm{w}}\right)=|\mathrm{n}(\vec{\mathrm{w}})|^2$ is the noise power.

Finally, the third term, $\tilde{\gamma}_{\mathrm{Scat}}(\vec{\mathrm{w}})$, reflects the phase stability of the scatterer under the different incidence angles induced by the interferometric baseline. After range and azimuth spectral filtering [34], $\tilde{\gamma}_{\mathrm{Scat}}(\vec{\mathrm{w}})$ reduces to the volume decorrelation contribution $\tilde{\gamma}_{\mathrm{Vol}}(\vec{\mathrm{w}})$ [7], [35]

$$\tilde{\gamma}_{\mathrm{Vol}}\left(\kappa_{\mathrm{z}},\vec{\mathrm{w}}\right)=\frac{\int_{\mathrm{z}_0}^{\mathrm{z}_0+\mathrm{h_V}}\mathrm{F}\left(\mathrm{z},\vec{\mathrm{w}}\right)\,\exp\left(\mathrm{i}\kappa_{\mathrm{Z}}\,\mathrm{z}\right)\mathrm{dz}}{\int_{\mathrm{z}_0}^{\mathrm{z}_0+\mathrm{h_V}}\mathrm{F}\left(\mathrm{z}\right)\,\mathrm{dz}}. \tag{4}$$

$\mathrm{F}(\mathrm{z},\vec{\mathrm{w}})$ (where z indicates the vertical axis/position) is the vertical reflectivity function (also referred as the vertical reflectivity profile) and expresses the vertical distribution of scatterers seen by the interferometer. Accordingly, $\mathrm{F}(\mathrm{z},\vec{\mathrm{w}})$ depends on the frequency and polarisation of the interferometer as well as on the interferometric acquisition geometry. The upper bound of $\mathrm{F}(\mathrm{z},\vec{\mathrm{w}})$ is given by $\mathrm{z}_0+\mathrm{h_V}$ which in the case of a forest scatterer corresponds to the (top) forest height. The lower bound of $\mathrm{F}(\mathrm{z},\vec{\mathrm{w}})$ is given by the reference height z_0 associated with the location of the underlying ground. The vertical (interferometric) wavenumber κ_{z} is defined as

$$\kappa_{\mathrm{z}}=\mathrm{m}\frac{2\pi}{\lambda}\frac{\Delta\theta}{\sin\left(\theta_0\right)} \tag{5}$$

where θ_0 is the nominal incidence angle, λ the wavelength, and $\Delta\theta$ the change of the incidence angle induced by the spatial baseline. The factor m accounts for the acquisition mode: $\mathrm{m}=2$ for monostatic acquisitions and $\mathrm{m}=1$ for bistatic acquisitions. In conventional interferometric applications, κ_{z} expresses the sensitivity of the interferometric phase to (terrain) height variations and is often expressed by the so called height of ambiguity HOA: $=2\pi/\kappa_{\mathrm{z}}$, i.e., the height that corresponds to the interferometric phase of 2π. In the context of (4), κ_{z} maps $\mathrm{F}(\mathrm{z},\vec{\mathrm{w}})$ to $\tilde{\gamma}_{\mathrm{Vol}}(\vec{\mathrm{w}})$ determining the sensitivity of the interferometer to a given $\mathrm{F}(\mathrm{z},\vec{\mathrm{w}})$ and especially to a given $\mathrm{h_V}$.

III. Forest Height Inversion

Equation (4) allows the estimation of $\mathrm{F}(\mathrm{z},\vec{\mathrm{w}})$ (and of the associated parameters as, for example, the forest height) from measurements of $\tilde{\gamma}_{\mathrm{Vol}}(\kappa_{\mathrm{z}},\vec{\mathrm{w}})$ performed at different spatial baselines κ_{z} and/or different polarisations $\vec{\mathrm{w}}$. One way to do so is to parameterize $\mathrm{F}(\mathrm{z},\vec{\mathrm{w}})$ into a set of geometrical and

scattering/propagation parameters and then to use $\tilde{\gamma}_{\mathrm{Vol}}(\kappa_z, \vec{w})$ measurements to estimate these parameters by inverting (4). For a robust inversion, the number of parameters used to parameterize $F(z, \vec{w})$ has to be balanced by the number of available $\tilde{\gamma}_{\mathrm{Vol}}(\kappa_z, \vec{w})$ measurements.

For forest applications, two-layer models have been proven to be sufficient (in terms of robustness and performance) to parameterize $F(z, \vec{w})$. While at lower frequencies, as at L- and P-band, the layers are considered continuously extended, at higher frequencies [7]–[9], such as at C- and even more at X-band, models with horizontally or vertically discontinuous layers have also been successfully used to describe interferometric measurements of corresponding forests [36]–[38]. In the following, we consider continuously extended layers. Accordingly, $F(z, \vec{w})$ consists of an extended vegetation (volume) component $f_V(z, \vec{w})$ and a Dirac-like component $m_G(\vec{w})\delta(z - z_0)$ that accounts for the scattering contribution(s) occurring on (or with) the underlying ground (i.e., direct surface and dihedral vegetation-surface contributions)

$$F\ (z, \vec{w}) = f_V\ (z, \vec{w}) + m_G\ (\vec{w})\, \delta\,(z - z_0) \tag{6}$$

where $m_G(\vec{w})$ is the ground scattering amplitude. Substituting (6) in (4) leads to

$$\tilde{\gamma}_{\mathrm{Vol}}\ (\kappa_z, \vec{w}) = \exp(i\,\varphi_0)\, \frac{\tilde{\gamma}_{V0}\,(\kappa_z, \vec{w}) + m\,(\vec{w})}{1 + m\,(\vec{w})} \tag{7}$$

where $\varphi_0 = \kappa_Z\, z_0$ is the phase related to the underlying ground height z_0 and

$$\tilde{\gamma}_{V0}\ (\kappa_z, \vec{w}) = \frac{\int_0^{z_V + h_V} f_V\,(z, \vec{w}) \exp(i\kappa_Z\, z)\, dz}{\int_0^{h_V} f_V\,(z, \vec{w})\ dz} \tag{8}$$

is the volume only coherence and $m(\vec{w}) = m_G(\vec{w}) / \int_0^{h_V} f_V(z, \vec{w})\, dz$ is the effective ground-to-volume (amplitude) ratio.

Different models have been proposed for modeling the vertical distribution of scatterers in the vegetation layer $f_V(z, \vec{w})$ including exponential, linear, Gaussian, and polynomial formulations. A widely used approach is to assume an exponential distribution of scatterers

$$f_V\ (z, \vec{w}) = m_V\ (\vec{w})\ \exp\left(2\sigma\,(\vec{w})\, z / \cos(\theta_0)\right) \tag{9}$$

where $f_V(z, \vec{w})$ is described by an exponential defined by a single parameter, namely the exponential rate $\sigma(\vec{w})$. At higher frequencies, $\sigma(\vec{w})$ can be interpreted as a mean extinction value for the vegetation layer associated with the "attenuation rate" of the profile so that $\sigma(\vec{w})$ is often expressed in [dB/m]. In the case of a Random Volume $\sigma\,(\vec{w}) = \sigma$ becomes polarization independent so that

$$f_V\ (z, \vec{w}) = f_V\ \ (z) = m_V\ (\vec{w})\ \exp\left(2\sigma z / \cos(\theta_0)\right) \tag{10}$$

and the total vertical distribution of scatterers $F(z, \vec{w})$ is

$$F\ (z, \vec{w}) = m_V\ (\vec{w})\ \exp\left(2\sigma z / \cos(\theta_0)\right) + m_G\,(\vec{w})\, \delta\,(z - z_0)\,. \tag{11}$$

The model of (11) known as the Random Volume over Ground [7] model comprises four unknowns: the forest height h_V, the extinction coefficient σ, the phase term φ_0 associated with the reference height z_0, and the polarization-dependent ground-to-volume ratio $m(\vec{w})$. The polarization-dependent volume scattering amplitude $m_V(\vec{w})$ cancels out when forming the interferometric coherence [see (8)] leading to a polarization-independent volume only coherence expression.

The inversion of (11) using a single baseline requires the availability of quad-pol data but leads – when unconstrained – to non-unique solutions [39], [40]. Assuming a zero-ground-to-volume amplitude ratio, i.e., $m\,(\vec{w}_V) = 0$, in at least one polarization $\vec{w}_V$ allows the unambiguous estimation of forest height. At the same time $m\,(\vec{w}_V) = 0$ allows a balanced inversion problem even in the case of dual-pol data [25].

The standard DEM mode of TanDEM-X is, however, a single-pol mode operated in HH (i.e., $\vec{w}_{HH}$) or VV (i.e., $\vec{w}_{VV}$) polarization. Assuming $m(\vec{w}_V) = 0$, that transforms (7) to

$$\tilde{\gamma}_{\mathrm{Vol}}\ (\kappa_z, \vec{w}) = \exp(i\,\varphi_0)\ \tilde{\gamma}_{V0}(\kappa_z, \vec{w}) \tag{12}$$

is not enough for obtaining a balanced inversion scenario as there are still three remaining unknowns, i.e., the forest height h_V, the extinction coefficient σ, and the phase term φ_0 against a (complex) interferometric volume coherence measurement $\tilde{\gamma}_{\mathrm{Vol}}(\vec{w}_{HH})$. In this case, the inversion relies on the additional assumptions or external information available.

There are two possible ways to force a balanced inversion problem from a single-channel interferometer. The first one is to use an external DTM to estimate the ground topographic phase $\exp(i\varphi_0)$. For this, the DTM is converted to a topographic phase term $\exp(i\varphi_{DTM}) = \exp(i\, h_{DTM}\, \kappa_Z)$. A remaining (constant) phase offset $\exp(i\varphi_{Off})$ between $\exp(i\varphi_{DTM})$ and $\tilde{\gamma}(\kappa_Z, \vec{w}_{HH})$ can be estimated by using a reference point (as a corner reflector or a bare area with high coherence) so that $\exp(i\varphi_0) = \exp(i\varphi_{Off})\ \exp(i\varphi_{DTM})$. In this way, (9) can then be inverted for forest height h_V and extinction σ by means of

$$\min_{h_v, \sigma} \|\tilde{\gamma}_{\mathrm{Vol}}\,(\kappa_Z, \vec{w}_{HH}) \exp(-i\varphi_0) - \tilde{\gamma}_{V0}\,(\kappa_Z, h_V, \sigma)\,\|. \tag{13}$$

The second way is to fix the extinction coefficient to a certain value $\sigma : = \sigma_0$, that is equivalent to fix $f_V(z, \vec{w})$ (and consequently $F(z, \vec{w})$). This leads to a balanced inversion problem

$$\min_{h_v, \varphi_0} \|\tilde{\gamma}_{\mathrm{Vol}}\,(\kappa_Z, \vec{w}_{HH}) - \tilde{\gamma}_{V0}\,(\kappa_Z, h_V, \varphi_0)\,\|. \tag{14}$$

The special case of $\sigma := 0$ dB/m corresponds to a uniform distribution of scatterers and leads to the characteristic sinc-decorrelation function

$$\tilde{\gamma}_{\mathrm{Vol}}\ (\kappa_z, \vec{w}) = \exp\left(i\kappa_z\, z_0 + i\frac{\kappa_z\, h_V}{2}\right) \mathrm{sinc}\left(\frac{\kappa_z\, h_V}{2}\right) \tag{15}$$

where $\mathrm{sinc}\,(x) = \sin(x)/x$. In this case, the volume coherence at a given baseline depends only on the forest height h_V, and the ground topography $\varphi_0 = \kappa_z\, z_0$. The phase center is located at half the forest height. This reduces the estimation of forest height to a single parameter estimation by means of (15) and can be performed using the absolute value of the volume coherence.

IV. Lidar Waveform Data

Large footprint, full waveform lidars as NASA's airborne Land, Vegetation, and Ice Sensor (LVIS) [41] transmit short

laser pulses to illuminate an area on the ground and receive the reflected distribution of (light) energy, known as the waveform, as a function of time. Accordingly, the received waveform depends directly on the 3D distribution of the intercepted vegetation elements within the footprint [42]. The reflected (i.e., backscattered) intensity from a vegetation layer of thickness (i.e., height) $\mathrm{h_V}$ located over a reference elevation $\mathrm{z_0}$ – ignoring for simplicity the propagation through the atmosphere and assuming a penetration until the ground level $\mathrm{z_0}$ – can be modeled as

$$\mathrm{I\,(x,y,z)\ = I_0 \int_{z_0}^{z_0+h_V} \iint \sigma\,(x,y,z)\cdot e^{-\tau(z-z_0)} dydxdz} \tag{16}$$

where $\sigma(x, y, z)$ is the volumetric reflection of the vegetation layer, τ the volumetric extinction coefficient that accounts for the two-way attenuation within the vegetation layer. Assuming for simplicity a constant weighting across the footprint, the horizontal dependency can be dropped and the received waveform $\mathrm{P(z)}$ is obtained by the convolution of the reflected intensity with the system pulse shape p(z)

$$\mathrm{P\ (z) = p\,(z) \otimes I\,(z)\,.} \tag{17}$$

It is clear that lidar waveforms $\mathrm{P(z)}$ and X-band vertical reflectivity profiles $\mathrm{F(z,\vec{w})}$ are not the same because of the difference in frequency and acquisition geometry. However, the high attenuation at both frequencies makes both $\mathrm{P(z)}$ and $\mathrm{F(z,\vec{w})}$ sensitive to the geometric architecture of the canopy reflectivity profiles $\mathrm{F(z,\vec{w})}$. However, the high attenuation at both frequencies makes both $\mathrm{P(z)}$ and $\mathrm{F(z,\vec{w})}$ sensitive to the geometric architecture of the canopy. This introduces a certain similarity between $\mathrm{P(z)}$ and $\mathrm{F(z,\vec{w})}$, especially when both are measured at the same or similar spatial resolution, which is explored in the following. In this sense, the use of the lidar waveforms P(z), normalized to unit height, in (4)

$$\tilde{\gamma}_{\mathrm{Vol}}\ (\kappa_z, \vec{w}) = \frac{\int_{z_0}^{z_0+h_V} \mathrm{P\,(z)\ exp\,(i\kappa_Z\,z)\,dz}}{\int_{z_0}^{z_0+h_V} \mathrm{P\,(z)\ dz}} \tag{18}$$

to estimate forest height by inverting single-baseline single-polarimetric interferometric volume coherence measurements by TanDEM-X is attempted.

V. Experimental Data

The AfriSAR campaign was deployed in 2015 and 2016 as a joint effort among space agencies over the African tropical forests of Gabon [43]–[45]. The objective of the campaign was to perform interferometric and tomographic SAR as well as lidar waveform and ground measurements for the development, calibration, and validation of tropical forest structure and biomass estimation algorithms relevant in the context of future spaceborne SAR and Lidar missions. One of the main test sites of AfriSAR was in the Lopé National Park, consisting of monsoon forest and savannah landscapes. The terrain is hilly, with many local slopes steeper than 20°. The maximum tree height exceeds 50 m in many stands. The forest (above ground) biomass ranges between 10 t/ha at savanna areas up to ∼400 t/ha at mature forest stands. For this work, the data collected by TanDEM-X and LVIS, NASA's LVIS, an airborne, wide-beam full-waveform lidar system [44]–[47], in the framework of AfriSAR are used.

The TanDEM-X data have been acquired on January 25, 2016, in a strip-map bistatic single-pol descending mode at HH-polarization at 44.5° (nominal) incidence angle and (mean) vertical wavenumber $\mathrm{k_z} = 0.1\ \mathrm{rad/m}$ corresponding to a Height of Ambiguity $HoA = 62.8$ m.

In February 2016, LVIS was flown onboard NASA's Langley B200 aircraft over Lopé acquiring full waveforms over footprints with a mean diameter of approximately 22 m in a continuous way. From these, the RH100 map (i.e., the height in meters relative to the ground level at which 100% of the waveform energy occurs), as well as the DTM are derived.

Both TanDEM-X (i.e., the interferometric volume coherence component obtained after the compensation of SNR and other system decorrelation contributions [48] and LVIS data (i.e., RH100 and DTM) are resampled to 10×10 m grid and projected to UTM coordinates. Fig. 1 shows from left to right the LVIS RH100 map, the TanDEM-X HH backscatter power map, and the LVIS DTM in UTM coordinates. Only the areas covered by LVIS are shown.

VI. Experimental Results

The different inversion schemes discussed in Section IV are now applied to the experimental data introduced in Section V. First, acting as a reference, the inversion under the no ground assumption, i.e., $\mathrm{m_G(\vec{w}_V) = 0}$ and using a zero extinction coefficient, i.e., $\sigma := 0$ is performed. The obtained results and their comparison against the Lidar reference data are shown in the first row of Fig. 2: On the left: the obtained forest height map, in the middle: the height difference map between estimated and the reference (i.e., LVIS Lidar) heights and on the right: the (normalized) validation plot are shown. The obtained height estimates are clearly underestimated for heights larger than 30 m. The overall root mean square error is $\mathrm{RMSE} = 16.7$ m and the correlation coefficient $r^2 = 1 - \sum (y - \tilde{y})^2 / \sum (y - \bar{y})^2 = -4.58$ where y is the height estimate, $\bar{y}$ is the mean height estimate, and $\tilde{y}$ is the reference height [49].

Next, the inversion using the individual LVIS waveforms is performed. For each volume coherence sample of the $20 \times 20\ \mathrm{m^2}$ grid, the corresponding height normalized LVIS waveform P(z) is used to approximate the reflectivity function by means of (18). Also here the inversion was performed by using the absolute value of the volume coherence only in order to remove the topographic dependency. The results are shown in the second row of Fig. 2. The performance is improved with respect to the height estimates obtained using the zero-extinction reflectivity profile with an RMSE $= 13.85$ *m* and $r^2 = -1.89$. But also here the heights higher than 35 m are underestimated. By looking at the height difference map, it becomes clear that the underestimation occurs on particular forest stands and is not correlated with topographic slopes.

Fig. 3 zooms into such an underestimated stand: on the bottom plot: the fine beam LiDAR height image and on the top - the TanDEM-X volume coherence map scaled from 0 (black) to 1 (white) are shown. The LiDAR height image indicates a dense

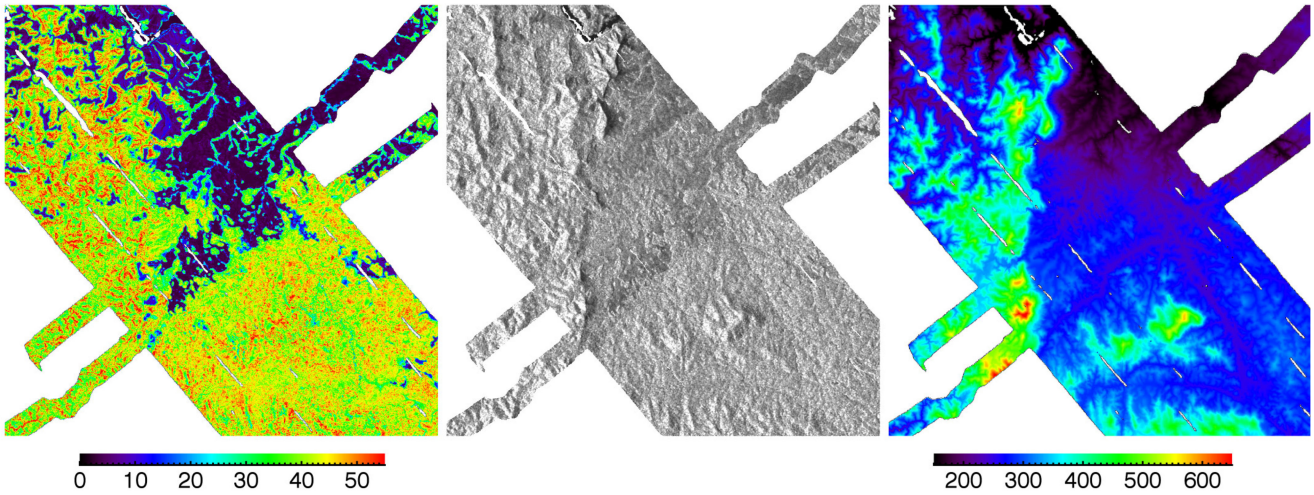

Fig. 1. Lopé site. From left to right: LVIS RH100 [m], TanDEM-X HH power, and LVIS DTM [m] in UTM coordinates. Only the areas covered by the LVIS measurements are shown.

forest stand while the high (almost surface-like) coherence level indicates a very limited penetration comparable to the nearby surface. This makes clear that the main reason for the underestimation is the limited penetration at X-band that prevents from "seeing" the whole (vertical) forest extent.

It is well known that the underestimation of forest height can be compensated by using the information of the underlying ground topography in form of an (externally) available DTM. The conventional approach for this correction is to convert the DTM height $\mathrm{h_{DTM}}$ to a topographic phase component $\varphi_{\mathrm{DTM}} = \mathrm{h_{DTM}}\ \kappa_{\mathrm{Z}}$ and subtract it from the interferometric phase of the (complex) volume coherence [25]. This approach is the most accurate way to compensate the underestimation of tall/dense stands, however, it requires an accurate DTM as any DTM error propagates directly to the height error budget. Here, an alternative DTM-based approach to handle the underestimation problem is proposed, which may also be (more) robust against DTM inaccuracy. The affected stands/samples are identified and "filtered out" by means of a simple filter defined using in this case the available LVIS DTM. Accordingly, we consider only the areas where the estimated forest height is larger than the phase center height, i.e., the height difference between the TanDEM-X phase center location and the topographic ground (DTM) height $\mathrm{H_{DTM}}$

$$\mathrm{h_v} \geq a_T \frac{\varphi - \varphi_{\mathrm{DTM}}}{\mathrm{k_z}} \tag{19}$$

where $\varphi_{\mathrm{DTM}} = \mathrm{k_z}\ \mathrm{H_{DTM}}$ and a_T is a threshold parameter. The results after applying the underestimation filter using $a_T = 1$ are shown in the third row of Fig. 2. The filter removes 2.5% of the height estimates. The height underestimation of the tall stands is clearly reduced since the filter removed most of the cases of insufficient penetration. It is important to note that the threshold a_T in (19) determines the performance of the underestimation compensation. Higher thresholds (up to $a_T = 1.2$) compensate underestimation better at the price of removing a larger number of samples. Lower thresholds (up to $a_T = 0.8$) keep more samples but compensate the underestimation less effectively.

Finally, the quality of the available DTM plays also a role in the threshold selection. A more conservative (e.g., higher) threshold also compensates – up to a certain degree – for larger DTM errors (e.g., variance). In other words, a less accurate DTM can be used at the expense of a higher amount of removed height samples.

For comparison, the underestimation filter using $a_T = 1$ is also applied to the height estimates obtained using the zero-extinction reflectivity profile removing about 18.7% of the estimates. The results are shown in the fourth row of Fig. 2. The performance with RMSE $= 9.3$ m and $r^2 = 0.23$ is now improved with respect to the "unfiltered" estimates but inferior with respect to the inversion using the LVIS waveforms.

The remaining underestimation of the taller stands is caused by the insufficiency of the assumed zero-extinction reflectivity profile to describe the real underlying reflectivity profile: the actual ground contribution in the TanDEM-X reflectivity is expected to be significantly smaller than the reflectivity at heights closer to the top while the zero-extinction reflectivity profile assumes the same reflectivity across the whole height range. Having said this, it is also important to look at the lower height range (i.e., below 20 m) of the validation plot where both approaches overestimate. Part of the overestimation in this lower height region is attributed to the inherent residual non-volumetric decorrelation contribution. But there is more than this, as the performance of the zero-extinction reflectivity profile is better than the performance achieved using the LVIS waveforms. The reason for this is that the LVIS waveforms are not the same as the TanDEM-X reflectivity profiles. Even though both profiles are in a similar (but not identical) way predominantly defined by the geometric properties/architecture of the canopy (due to the high frequency range in which both systems operate and the high spatial resolutions) the different

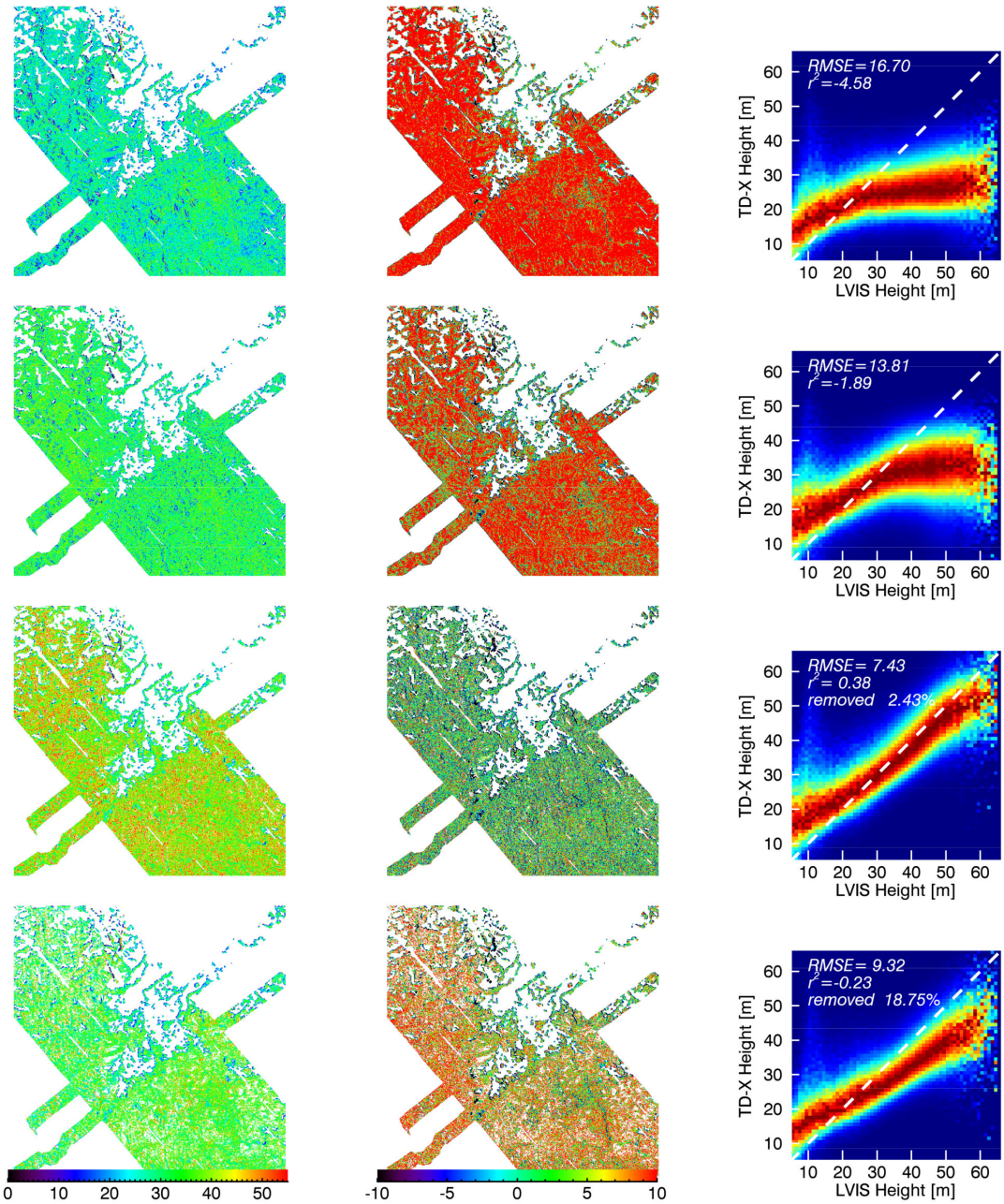

Fig. 2. From left to right: forest height inverted from TanDEM-X coherence, the inversion error with respect to LVIS CHM reference and the performance validation plot using: zero extinction profile (first row), individual LVIS waveforms (second row), individual LVIS waveforms for samples which satisfied the criteria (19) with $\boldsymbol{a_T} = 1$ (third row), and zero extinction profile for samples which satisfied the criteria (19) with $\boldsymbol{a_T} = 1$ (fourth row).

acquisition geometries induce significant differences especially when it comes to lower/sparser forest stand conditions. The nadir-looking LVIS geometry is responsible for a larger ground contribution compared to the TanDEM-X reflectivity where the side-looking geometry implies a larger way through the forest canopy and, thus, a stronger attenuation of the ground scattering contribution. Exactly this larger ground contribution in the LVIS waveforms (relative to the underlying X-band ground contribution) causes the overestimation when using the LVIS waveforms compared to the results achieved assuming a zero-extinction reflectivity profile.

VII. "Mean" Profile

In the previous section, the use of LVIS waveforms P(z) to approximate the TanDEM-X reflectivity function in the context of forest height inversion is discussed and demonstrated. This approach can be followed everywhere where lidar data are available. However, usually, the available lidar data do not cover the whole TanDEM-X scene. In order to extend such a lidar-supported TanDEM-X data inversion also to areas where lidar data are not available, the concept of a "mean" profile used for the whole scene is attempted [50], [51].

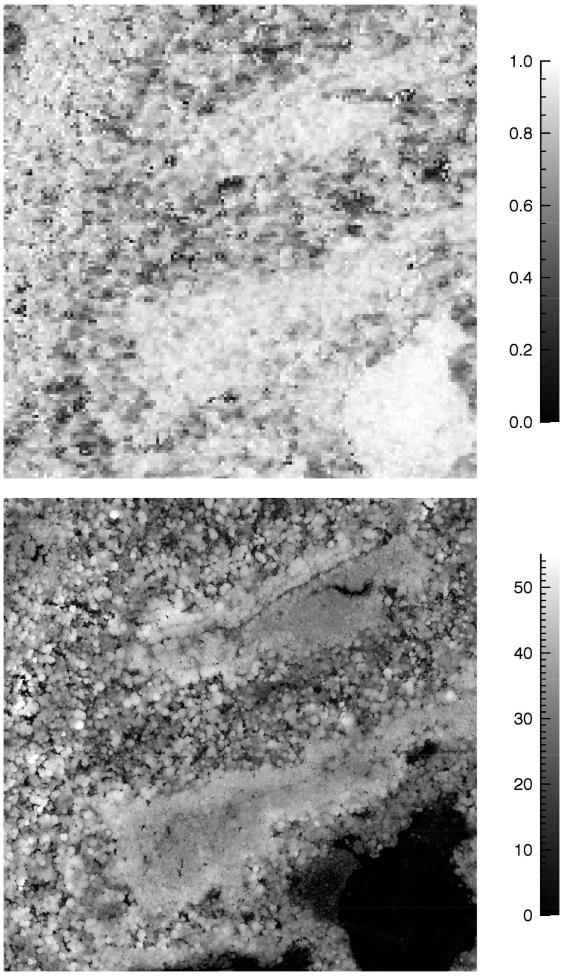

Fig. 3. Top plot: TanDEM-X volume coherence approaching values in the dense forest similar to those on surface, indicating low penetration zone. Bottom plot: Forest height measured by fine-beam LiDAR (1-m resolution) in the dense forest region.

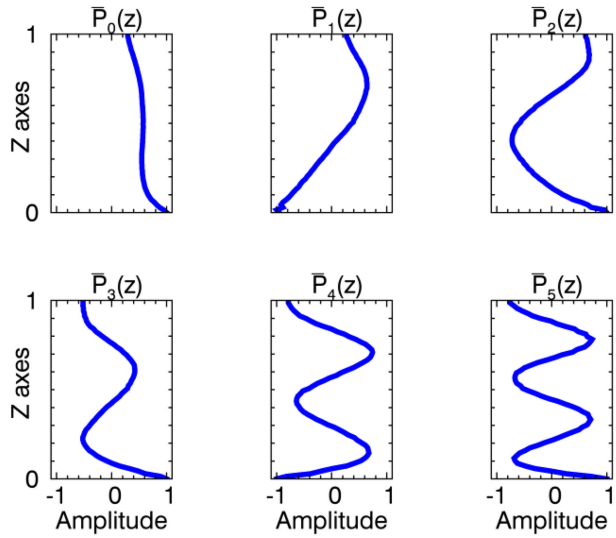

Fig. 4. First six eigenfunctions of the profile covariance matrix.

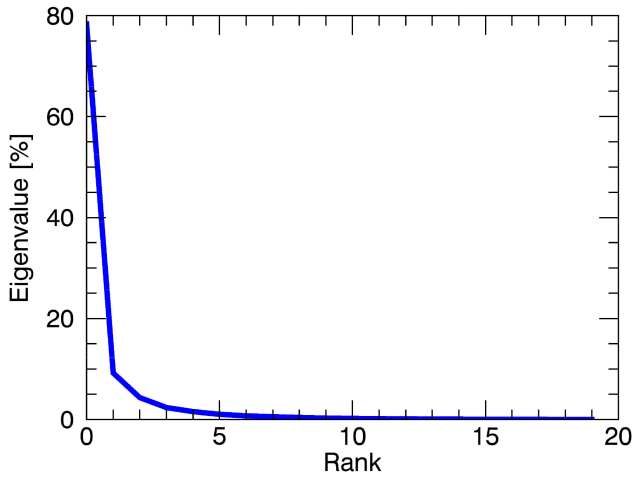

Fig. 5. Spectrum of eigenvalues of the profile covariance matrix.

The first step for obtaining such a "mean" profile from the available lidar waveforms is the formation of the so-called profile matrix. The available lidar waveforms $P_i(z)$ are normalized to unit height, resampled to a common number of height samples between 0 and 1, and stacked as columns of the profile matrix [P].

From the profile matrix, a covariance matrix is formed and diagonalized

$$[\mathrm{R}] = [P]\,[P]^T = [U]\,[\Lambda]\,[U]^T. \tag{20}$$

The diagonal matrix $[\Lambda]$ contains the positive real eigenvalues of [R] while the columns of $[U]$ are given by the orthogonal eigenfunctions of [R] $\bar{P}_i(z)$. Fig. 4 shows the first six eigenfunctions while Fig. 5 illustrates the spectrum of the eigenvalues obtained using all available LVIS waveforms when forming [P]. An important result is that already the first eigenvalue represents almost 80% of the total profile power (i.e., the trace of $[\Lambda]$ given by the sum of all eigenvalues) while the first five eigenvalues represent more that 95%. This indicates that already a small number of eigenfunctions is sufficient for a widely accurate profile representation and/or reconstruction. Higher order eigenvalues (and thus the associated eigenfunctions) become less significant for the reconstruction of the profile.

The obtained eigenfunctions can be used to build up the "mean" profile by means of linear combination

$$F_m(z) = \sum_{i=1}^{\mathrm{N}} a_i \bar{P}_i(z). \tag{21}$$

Note that (21) is very similar to the concept of orthogonal functions for describing the vertical radar reflectivity as proposed in [10] but addressed in terms of lidar waveforms rather than Lagrange polynomials. In the following, only the first eigenfunction $F_m(z) = \bar{P}_1(z)$ is used. Using $F_m(z)$ in (4) and taking the absolute coherence value reduces the forest height inversion to a single parameter estimation. The same mean profile is used to invert the whole scene. The underestimation filter of (19) with $a_T = 1$ is applied on the forest height estimates

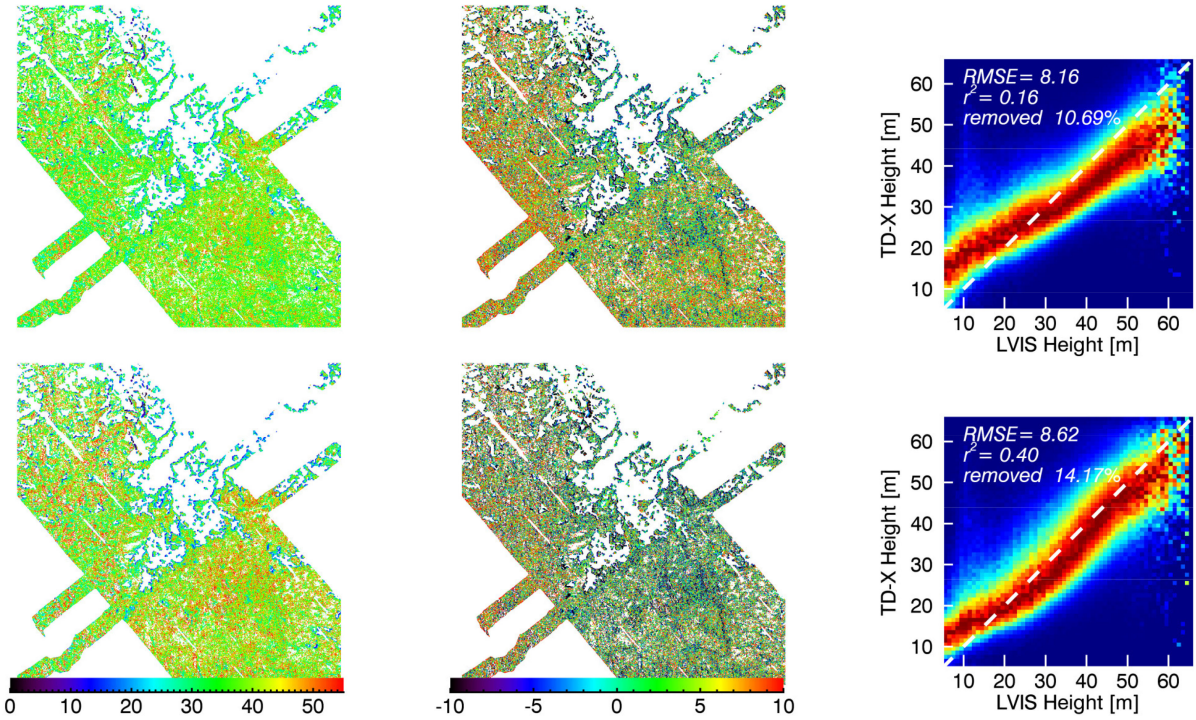

Fig. 6. From left to right: Forest height inverted from TanDEM-X coherence for samples that satisfied the criteria (19) with $\boldsymbol{a_T} = 1$, the inversion error with respect to LVIS CHM reference and the performance validation plot using: the representative profile (top row) and a representative profile for two height classes (bottom row).

obtained removing about 10.6% of the estimates. The results obtained (after filtering) are shown in the first row of Fig. 6: from left to right the filtered forest height map, the height difference map with respect to the reference LVIS forest heights and the (normalized) validation plot. The obtained height estimates are surprisingly good with $\mathrm{RMSE} = 8.16$ and $r^2 = 0.16$.

A comparison with the validation plot obtained when using for each coherence sample the individual LVIS waveform (shown in the third raw of Fig. 2.) makes clear that the underestimation of the taller stands obtained using the "mean" profile is not due to the penetration limitations, but rather to the discrepancy between the "mean" profile and the actual underlying reflectivity profile. The "mean" profile seems to overestimate the actual ground contribution in the TanDEM-X reflectivity.

Nevertheless, the results suggest that the use of a single profile still allows a reasonable forest height estimation performance. The quality of the final performance depends on the structural heterogeneity of the individual scene. At the same time, the estimation of the eigenfunctions and, thus, of the "mean" profile appears (very) robust with respect to the number of available waveforms. Even only 10% of the waveforms lead to practically the same eigenfunctions and eigenvalues (assuming a relative homogeneous "thinning" of samples). In this sense, a homogeneous distribution of waveforms across the different stand structures within the scene is more important than a very high number of waveforms.

One way to improve the performance is to account for the change of the "mean" profile at the different height classes. This can be done by estimating the "mean" profile within different height intervals and interpolating the obtained solution spaces. For example, the representative (height normalized) profile obtained accounting only for forest heights below 25 m is shown in Fig. 7 by the blue curve and the profile accounting only for forest heights above 40 m – by the green curve. The ground contribution (accounted relative to the canopy contribution) is, as expected, large(r) for the lower height range and decreases significantly in the higher height range. In order to avoid any discontinuity in the solution space obtained when using the

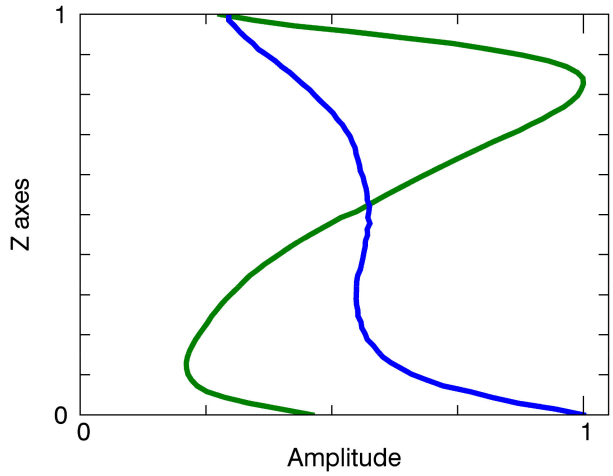

Fig. 7. Zero-order eigenfunction derived for the tree classes from 20 to 25 m (blue curve) and from 40 to 45 m (green curve).

two "mean" profiles in (15), the transition from the one height range to the other is interpolated over a sufficiently wide height range; in this case, between 25 and 40 m. The obtained results (after filtering that removes about 14% of the height estimates) are finally shown in the second row of Fig. 6. The overall performance is improved (even if the overall RMSE $= 8.62$ is slightly worse) as the correlation increases to $r^2 = 0.40$ and the underestimation of the taller stand is compensated.

VIII. Discussion and Conclusion

Model-based forest height inversion from Pol-InSAR data relies on the realistic parameterization of the underlying (vertical) radar reflectivity function. Interferometric coherence measurements at different polarizations and/or spatial baselines are then used to recover the reflectivity parameterization or parts of it. In the context of interferometric TanDEM-X - especially in the global single pol DEM mode, the limited dimensionality of the observation space does not allow the reconstruction of even very primitive vertical reflectivity parameterizations (as for example a vertically exponential decreasing reflectivity). Thus, in order to explore the inherent sensitivity of the interferometric TanDEM-X coherence to the vertical forest structure, additional information is required. This can be in form of *a priori* information (for example in form of a DTM) or by means of complementary (ground-, air-, or space-borne) remote sensing measurements.

The use of lidar measurements to support the inversion of structure-based interferometric TanDEM-X coherence is already investigated in a number of studies. A given similarity of lidar and TanDEM-X measurements, induced by the high sensitivity to the geometrical attributes/architecture of the canopy, the high attenuation rates and the high spatial resolution common to both configurations, supports such approaches.

In this work, the use of lidar waveforms to directly approximate TanDEM-X reflectivity is proposed. The adequate performance achieved should not imply that the lidar waveforms equal TanDEM-X reflectivity. There can be significant deviations primarily induced by the different acquisition geometries (nadir-looking lidar vs side-looking TanDEM-X) especially when it comes to lower/sparser but also tall forest stands. The nadir looking LVIS geometry results in larger ground contributions compared to the TanDEM-X reflectivity where due to side-looking geometry, the paths through the forest canopy are larger leading to weaker ground scattering contributions. However, even if not the same, lidar waveforms appear a sufficiently good approximation of TanDEM-X reflectivity for forest height estimation.

The underestimation of forest heights as a result of limited penetration at X-band shows up clearly as a serious error contribution in tropical (and probably not only) forests vegetation especially for tall and/or dense forest conditions. As already discussed, the best way to account for it is to use an (accurate) external DTM. This allows us to obtain unbiased (with respect to penetration) forest height estimates for each coherence sample. The accuracy of the DTM has to be on the order of the forest height accuracy aimed at. An alternative approach is proposed and implemented here relying on comparing the obtained forest height estimates against the height of the phase center: forest height estimates below a given threshold are removed. The advantage – when compared to the DTM approach – is that a lower accuracy DTM can be used paying the price of less valid samples.

Finally, the use of a single "mean" reflectivity profile derived from the available lidar waveforms is proposed. Also in this case, the achieved performance is remarkably good even if the limitations of using a single fixed profile across stands with the very different structure are evident. One step in improving this is attempted by accounting for different "mean" profiles for different height classes with a given success. However, this is probably not the best possible way to overcome this problem as the definition of the necessary height ranges for an optimal inversion performance may vary with forest conditions.

Nevertheless, it is important to realize that, in general, the forest height is the main contribution to interferometric volume coherence, while the effect of the shape of the (vertical) reflectivity is weaker, but still significant enough to have a decisive impact on the achieved performance. Accordingly, there is a performance tradeoff between the ability to adapt the vertical reflectivity model to the local stand conditions and the knowledge required to do this. This knowledge can be integrated into the inversion problem itself in terms of additional unknown parameters or provided by/derived from other forest structure measurements as attempted in this work.

Acknowledgment

The authors would like to thank the anonymous reviewers for their thoughtful review and valuable comments. The lidar AfriSAR data sets were provided by the Land, Vegetation, and Ice Sensor (LVIS) Team in Code 61A at NASA Goddard Space Flight Center with support from the University of Maryland, College Park.

References

[1] P. Köhler and A. Huth, "Towards ground-truthing of spaceborne estimates of above-ground life biomass and leaf area index in tropical rainforests," *Biogeosciences*, vol. 7, no. 8, pp. 2531–2543, 2010.

[2] R. O. Dubayah *et al.*, "Estimation of tropical forest height and biomass dynamics using lidar remote sensing at la Selva, Costa Rica," *J. Geophys. Res., Biogeosciences*, vol. 115, 2010.

[3] R. Q. Thomas, G. C. Hurtt, R. O. Dubayah, and M. H. Schilz, "Using lidar data and a height-structured ecosystem model to estimate forest carbon stocks and fluxes over mountainous terrain," *Can. J. Remote Sens.*, vol. 34, pp. 351–363, 2008.

[4] G. C. Hurtt *et al.*, "Linking models and data on vegetation structure," *J. Geophys. Res., Biogeosci.*, vol. 115, 2010, Art. no. G00e10.

[5] M. A. Lefsky, "A global forest canopy height map from the moderate resolution imaging spectroradiometer and the geoscience laser altimeter system," *Geophys. Res. Lett.*, vol. 37, no. 15, 2010, Art. no. L15401.

[6] K. P. Papathanassiou and S. R. Cloude, "Polarimetric SAR interferometry," *IEEE Trans. Geosci. Remote Sens.*, vol. 36, no. 5, pp. 1551–1565, Sep. 1998.

[7] K. P. Papathanassiou and S. R. Cloude, "Single-baseline polarimetric SAR interferometry," *IEEE Trans. Geosci. Remote Sens.*, vol. 39, no. 11, pp. 2352–2363, Nov. 2001.

[8] R. N. Treuhaft and P. R. Siqueira, "The vertical structure of vegetated and surfaces from interferometric and polarimetric radar," *Radio Sci.*, vol. 35, no. 11, pp. 141–177, 2000.

[9] R. N. Treuhaft and S. R. Cloude, "The structure of oriented vegetation from polarimetric interferometry," *IEEE Trans. Geosci. Remote Sens.*, vol. 37, no. 5, pp. 2620–2624, Sep. 1999.
[10] S. R. Cloude, "Polarization coherence tomography," *Radio Sci.*, vol. 41, no. 4, 2006, Art. no. RS4017.
[11] F. Kugler, S.-K. Lee, and K. P. Papathanassiou, "Forest height estimation by means of Pol-InSAR data inversion: The role of the vertical wavenumber," *IEEE Trans. Geosci. Remote Sens.*, vol. 53, no. 10, Jun. 2015.
[12] I. Hajnsek, F. Kugler, S. Lee, and K. Papathanassiou, "Tropical forest parameter estimation by means of Pol-Insar: The INDREX II campaign," *IEEE Trans. Geosci. Remote Sens.*, vol. 47, no. 2, pp. 481–493, Feb. 2009.
[13] G. Krieger, K. P. Papathanassiou, and S. R. Cloude, "Spaceborne polarimetric SAR interferometry: Performance analysis and mission concepts," *EURASIP J. Appl. Sig. Process.*, vol. 20, pp. 3272–3292, 2005.
[14] A. Moreira *et al.*, "Tandem-L: A highly innovative bistatic SAR mission for global observation of dynamic processes on the earth's surface," *IEEE Geosci. Remote Sens. Mag.*, vol. 3, no. 2, pp. 8–23, Jun. 2015.
[15] S. Quegan *et al.*, "The European space agency BIOMASS mission: Measuring forest above-ground biomass from space," *Remote Sens. Environ.*, vol. 227, pp. 44–60, 2019.
[16] S. K. Lee, F. Kugler, K. P. Papathanassiou, and I. Hajnsek, "Multi-baseline Pol-InSAR forest height estimation in the presence of temporal decorrelation," in *Proc. Eur. Conf. Synthetic Aperture Radar*, 2010, pp, 1–4.
[17] S. K. Lee, F. Kugler, K. P. Papathanassiou, and I. Hajnsek, "Quantification of temporal decorrelation effects at L-band for polarimetric SAR interferometry applications," *IEEE J. Sel. Topics Appl. Earth Obs. Remote Sens.*, vol. 6, no. 3, pp. 1351–1367, Jun. 2013.
[18] M. Lavalle, M. Simard, and S. Hensley, "A temporal decorrelation model for polarimetric radar interferometers," *IEEE Trans. Geosci. Remote Sens.*, vol. 50, no. 7, pp. 2880–2888, Jul. 2012.
[19] G. Krieger *et al.*, "TanDEM-X: A satellite formation for high-resolution SAR," *IEEE Trans. Geosci. Remote Sens.*, vol. 45, no. 11, pp. 3317–3341, Nov. 2007.
[20] G. Krieger *et al.*, "TanDEM-X: A radar interferometer with two formation flying satellites," *Acta Astron.*, vol. 89, pp. 83–98, 2013.
[21] M. J. Soja, H. Persson, and L. M. H. Ulander, "Estimation of forest height and canopy density from a single InSAR correlation coefficient," *IEEE Geosci. Remote Sens. Lett.*, vol. 12, no. 3, pp. 646–650, Mar. 2015.
[22] H. J. Persson and J. E. S. Fransson, "Comparison between TanDEM-X and ALS based estimation of above ground biomass and tree height in boreal forests," *Scand. J. Forest Res.*, vol. 32, pp. 306–319, 2017.
[23] R. Treuhaft *et al.*, "Tropical-forest biomass estimation at X-Band from the spaceborne TanDEM-X interferometer," *IEEE Geosci. Remote Sens. Lett.*, vol. 12, no. 2, pp. 239–243, Dec. 2015.
[24] S. Solberg *et al.*, "Forest biomass change estimated from height change in interferometric SAR height models," *Carbon Balance Manage*, vol. 9, no. 5, 2014, Art. no. 5.
[25] F. Kugler, D. Schulze, I. Hajnsek, H. Pretzsch, and K. Papathanassiou, "TanDEM-X Pol-InSAR performance for forest height estimation," *IEEE Trans. Geosci. Remote Sens.*, vol. 52, no. 10, pp. 6404–6422, Oct. 2014.
[26] J. I. H. Askne, J. E. S. Fransson, M. Santoro, M. J. Soja, and L. M. H. Ulander, "Model-based biomass estimation of a hemi-boreal forest from multitemporal TanDEM-X acquisitions," *Remote Sens.*, vol. 5, pp. 5574–5597, 2013.
[27] M. Schlund *et al.*, "TanDEM-X data for aboveground biomass retrieval in a tropical peat swamp forest," *Remote Sens. Environ.*, vol. 158, pp. 255–266, 2015.
[28] H. J. Persson *et al.*, "Experiences from large-scale forest mapping of sweden using TanDEM-X data," *Remote Sens.*, vol. 9, no. 12, 2017, Art. no. 1253.
[29] H. J. Persson, M. J. Soja, J. E. S. Fransson, and L. M. H. Ulander, "National forest biomass mapping using the two-level model," *IEEE J. Sel. Topics Appl. Earth Observ. Remote Sens.*, vol. 13, pp. 6391–6400, 2020.
[30] G. Sun *et al.*, "Forest biomass mapping from lidar and radar synergies," *Remote Sens. Envrion.*, vol. 115, pp. 2906–2916, 2011.
[31] M. Brolly, M. Simard, H. Tang, R. O. Dubayah, and J. P. Fisk, "A lidar-radar framework to assess the impact of vertical forest structure on interferometric coherence," *IEEE J. Sel. Topics Appl. Remote Sens. Earth Observ.*, vol. 9, no. 12, pp. 5830–5841, Dec. 2016.
[32] W. Qi *et al.*, "Improved forest height estimation by fusion of simulated GEDI lidar data and TanDEM-X InSAR data," *Remote Sens. Environ.*, vol. 221, pp. 621–634, 2019.
[33] W. Qi and R. O. Dubayah, "Combining Tandem-X InSAR and simulated GEDI lidar observations for forest structure mapping," *Remote Sens. Environ.*, vol. 187, pp. 253–266, 2016.
[34] R. Bamler and P. Hartl, "Synthetic aperture radar interferometry," *Inverse Problems*, vol. 14, no. 4, pp. R1–R54, 1998.
[35] J. Askne, P. Dammert, L. Ulander, and G. Smith, "C-band repeat-pass interferometric SAR observations of the forest," *IEEE Trans. Geosci. Remote Sens.*, vol. 35, no. 1, pp. 25–35, Jan. 1997.
[36] M. Santoro, J. I. H. Askne, G. Smith, and J. E. S. Fransson, "Stem volume retrieval in boreal forests from ERS-1/2 interferometry," *Remote Sens. Environ.*, vol. 81, no. 1, pp. 19–35, 2002.
[37] J. I. H. Askne, J. E. S. Fransson, M. Santoro, M. J. Soja, and L. M. H. Ulander, "Model-based biomass estimation of a hemi-boreal forest from multitemporal TanDEM-X acquisition," *Remote Sens.*, vol. 5, no. 11, pp. 5574–5597, 2013.
[38] M. J. Soja, H. J. Persson, and L. M. H. Ulander, "Estimation of forest biomass from two-level model inversion of single-pass InSAR data," *IEEE Trans. Geosci. Remote Sens.*, vol. 53, no. 9, pp. 5083–5099, Sep. 2015.
[39] S. R. Cloude, *Polarisation: Applications in Remote Sensing*. Oxford, U.K.: Oxford Univ. Press, 2009.
[40] T. Flynn, M. Tabb, and R. Carande, "Coherence region shape extraction for vegetation parameter estimation in polarimetric SAR interferometry," in *Proc IEEE Int. Geosci. Remote Sens. Symp.*, 2002, pp. 2596–2598.
[41] J. B. Blair, D. L. Rabine, and M. A. Hofton, "The laser vegetation imaging sensor: A medium-altitude, digitisation-only, airborne laser altimeter for mapping vegetation and topography," *ISPRS J. Photogramm. Remote Sens.*, vol. 54, pp. 115–122, 1999.
[42] R. O. Dubayah and B. D. Jason, "Lidar remote sensing for forestry," *J. Forestry*, vol. 98, pp. 44–46, 2000.
[43] I. Hajnsek *et al.*, "Technical assistance for the development of airborne SAR and geophysical measurements during the AfriSAR campaign, Tech. Rep., ESA 4000114293/15/NL/CT. [Online]. Available: https://earth.esa.int/documents/10174/134665/AfriSAR-Final-Report
[44] M. Hofton, J. Blair, D. Rabine, C. Brooks, and H. Cornejo, "Canopy height and structure measurements of gabon from medium-footprint waveform lidar," in *Proc. IEEE Int. Geosci. Remote Sens. Symp.*, 2017.
[45] S. Erasmi, M. Semmler, P. Schall, and M. Schlund, "Sensitivity of bistatic TanDEM-X data to stand structural parameters in temperate forests," *Remote Sens.*, vol. 11, no. 24, 2019, Art. no. 2966.
[46] J. B. Blair and M. Hofton, "AfriSAR LVIS L1B geolocated return energy waveforms, version 1. Boulder, Colorado USA. NASA National Snow and Ice Data Center Distributed Active Archive Center," 2018, doi: 10.5067/ED5IYGVTB50Z.
[47] J. B. Blair and M. Hofton, "AfriSAR LVIS L2 Geolocated Surface Elevation Product, Version 1. Boulder, Colorado USA. NASA National Snow and Ice Data Center Distributed Active Archive Center," 2018, doi: 10.5067/A0PMUXXVUYNH.
[48] M. Martone *et al.*, "Coherence evaluation of TanDEM-X interferometric data," *ISPRS J. Photogramm. Remote Sens.*, vol. 73, pp. 21–29, Sep. 2012.
[49] T. O. Kvålseth, "Cautionary note about R_2," *Amer. Statist.*, vol. 39, pp. 279–285, 1985.
[50] A. Hannachi, I. T. Jolliffe, and D. B. Stephenson, "Empirical orthogonal functions and related techniques in atmospheric science: A review," *Int. J. Climatol.*, vol. 27, pp. 1119–1152, 2007.
[51] J. Kutzbach, "Empirical eigenvectors of sea-level pressure, surface temperature and precipitation complexes over north america," *J. Appl. Meteorol.*, vol. 6, no. 5, pp. 791–802, 1967.

Roman Guliaev received the B.Sc. degree in physics from Saint Petersburg State Polytechnic University, St Petersburg, Russia, in 2014 and M.Sc. degree in physics from the Friedrich-Alexander University (FAU) of Erlangen-Nuremberg, Germany, in 2018. He is currently working toward the Ph.D. degree with the Swiss Federal Institute of Technology, Zurich, Switzerland.

From 2016 to 2017, he worked with the Biosensing Laboratory in the Max-Planck Institute for the science of Light, Erlangen, Germany; from 2017 to 2018, he was with the Remote Sensing Group of FAU University. In 2019, he joined the Information Retrieval Research Group at the Microwaves and Radar Institute, German Aerospace Center (DLR), Wessling, Germany.

Victor Cazcarra-Bes was born in Barcelona, Spain, in 1985. He received the B.S. degree in sound and image engineering from the University of Alicante, Alicante, Spain, in 2007, the M.S. degree in telecommunication engineering from the University Miguel Hernández, Elche, Spain, in 2010, and the Ph.D. in environmental engineering from the Swiss Federal Institute of Technology, Zurich, Switzerland, in 2019.

Since 2014, he is with the Department of the Microwaves and Radar Institute at the German Aerospace Center (DLR) as a member of the Information retrieval research group. His main general interests are in the area of synthetic aperture radar, signal processing, and the development of new algorithms for forest applications.

Dr. Cazcarra-Bes in 2020, received the DLR Science Award.

Matteo Pardini (IEEE member) received the Ms.Eng. degree (*summa cum laude*) in telecommunication engineering and the Ph.D. degree in information engineering from the University of Pisa, Pisa, Italy, in 2006 and 2010, respectively.

In January 2010, he joined the Radar Concepts Department, Microwaves and Radar Institute, Deutsches Zentrum fur Luft- und Raumfahrt (DLR) in Oberpfaffenhofen, Weßling, Germany, as a Research Scientist, after a visiting research period from August to December 2009. In 2017, he was a Visiting Scientist with the Department of Geographical Sciences, University of Maryland, College Park, MD, USA. His research interests include synthetic aperture radar (SAR) tomographic and polarimetric interferometric processing for 3-D bio/geophysical information extraction over natural volumes (forest, agriculture, and ice), SAR mission design, and SAR mission performance analysis.

Dr. Pardini is the member of DLR's TanDEM-X and Tandem-L science teams. He was the recipient of the IEEE GRSS IEEE GRSS J-STARS Paper Award, in 2019 and the DLR Science Award, in 2020.

Konstantinos Papathanassiou (Fellow, IEEE) received the Dipl. Ing degree and the Dr. degree from the Technical University of Graz, Austria, in 1994 and 1999.

From 1992 to 1994, he was with the Institute for Digital Image Processing of Joanneum Research, in Graz, Austria. Between 1995 and 1999, he was with the Microwaves and Radar Institute (HR) of the German Aerospace Center (DLR) in Oberpfaffenhofen, Germany. From 1999 to 2000, he was an EU postdoctoral fellow with Applied Electromagnetics in St. Andrews, Scotland. Since October 2000, he is again with the Microwaves and Radar Institute (HR) of the German Aerospace Center (DLR). He is a Senior Scientist leading the Information Retrieval Research Group at DLR-HR. He has more than 60 peer-reviewed articles in international journals and of more than 300 contributions in international conferences and workshops. His main research interests include polarimetric and interferometric processing and calibration techniques, polarimetric SAR interferometry, and the quantitative parameter estimation from SAR data, as well as in SAR mission design and SAR mission performance analysis.

Dr. Papathanassiou is the member of DLR's TanDEM-X and Tandem-L science teams, JAXA's ALOS-PalSAR Cal-Val teams, ESA's BIOMASS Mission Advisory Group and JAXA's Carbon and Kyoto initiative and NASA's GEDI Mission Science Team. He was the recipient of the IEEE GRSS IGARSS Symposium Prize Paper Award, in 1998, the Best Paper Award of the European SAR Conference (EUSAR), in 2002, and the IEEE GRSS J-STARS Paper Award, in 2019. In 2002 and 2020, he received the DLR Science Award, in 2011 the DLR's Senior Scientist Award and was awarded the IEEE Fellow Award, in 2015 and DLR's Otto Lilienthal Award, in 2020.